Searching for Planets with SIM

Andrzej J. Maciejwski and Maciej Konacki
Toruń Centre for Astronomy, N. Copernicus University, Poland

September 10, 2000

Abstract

We present a theoretical analysis of the astrometric searches for extrasolar planets with the Space Interferometry Mission (SIM). We present a model for future astrometric measurements with SIM and and discuss the problem of a reliable estimation of orbital elements of extrasolar planets. We propose a new method of data analysis and present a numerical test of its application on simulated SIM astrometric measurements.

1 Introduction

The Space Interferometry Mission (SIM, see `http://sim.jpl.nasa.gov/`) will measure positions of stars with precision 4μas in the wide-angle mode and up to 1μas in the narrow-angle mode. This will give a possibility to study many fundamental astrophysical problems. However, the most important and challenging goals of SIM is astrometric detection of extrasolar planetary systems including Earth-like planets around stars from the solar neighborhood. High precision astrometry requires adequately elaborated models and methods of data analysis. Among others, it is important to develop techniques allowing reliable detection of planetary signatures and extraction of the orbital elements.

In this paper we present a model of SIM narrow-angle measurements and discuss its accuracy. Our simple model allows, among others, to analyze higher order effects which are neglected in classical astrometry. Moreover, it permits to understand well the nature of an astrometric signal.

We propose also a method called the Frequency Decomposition (FD) to detect planets and help to obtain their orbital elements. This method was successfully used for PSR 1257+12 timing observations [3] and 16 Cygni B radial velocity measurements [2]. The particular nature of the astrometric observations requires, however, some modifications of our original approach.

The astrometric signal is a superposition of several effects of different magnitude and a proper analysis of the observations requires at least rough a priori knowledge of how different effects contribute to the signal. However, these effects depend on the parameters (such as number of planets, their eccentricities) which are unknown in advance. So what we propose is a two-step analysis (1) FD to understand the basic properties of the signal (i.e determine the number of planets and approximate values of their orbital elements) and (2) a least-squares fit based on a proper model and the starting values of parameters derived from the previous step to refine the parameters and obtain their uncertainties.

The basic idea of FD is the following. With few exceptions (proper motion, long period planets) the processes contributing to the signal are periodic. Therefore, our astrometric signal can be successfully modeled as a multiple Fourier series plus a polynomial of certain degree (to account for the proper motion and long period planets). FD is a numerical algorithm to obtain the estimates of frequencies, amplitudes and phases of such model [3]. Full description of this method adopted to astrometric measurements can be found in [4], here we mention only that it is especially useful for multiple planetary systems where deciphering the number of planets may be tricky, e.g. two planets in circular 2:1 resonant orbits may mimic one planet in an eccentric orbit, see[1]; it is helpful while trying to determine whether we observe an astrometric displacement from a planet in 1-yr orbit or annual parallax, since the parallactic motion has its own specific Fourier expansion constrained by SIM orbit.

2 Modeling delays

SIM measures relative positions of stars using Michelson interferometers. A single measurement with SIM gives the projection of direction to the star $\mathbf{s}$ onto the interferometer baseline vector $\mathbf{B}$. The measured quantity is the optical pathlength delay between the two arms of the interferometer [5]

$$d = \mathbf{B} \cdot \mathbf{s} + c + \epsilon, \tag{1}$$

where c is the zero point of the metrology gauge and ϵ represents measurement uncertainty. The search for extrasolar planet is performed in the so called narrow angle mode where delays toward two stars (called target and reference) within 1° are measured and compared. For this kind of observation the measured quantity becomes the relative delay

$$D = \mathbf{B} \cdot (\mathbf{s}_1 - \mathbf{s}_2) + \epsilon, \tag{2}$$

where $\mathbf{s}_1$ and $\mathbf{s}_2$ are directions from SIM to the target and reference stars, respectively. Such narrow-angle measurement gives the angular separation between the stars and offers higher accuracy than many errors scale with the angular distance.

The direction to a star $\mathbf{S} = \mathbf{S}(t)$ from the Solar System Barycenter (SSB) is changing with time due to the proper motion and the presence of companions. We model these two effects in the following way

$$\mathbf{S}(t) = \mathbf{S}_0 + \delta\mathbf{S}_\mu(t) + \delta\mathbf{S}_{\mathrm{c}}(t), \tag{3}$$

where $\mathbf{S}_0$ is the direction towards the star at epoch t_0; $\delta\mathbf{S}_\mu(t)$ and $\delta\mathbf{S}_{\mathrm{c}}(t)$ describe changes due to the proper and orbital motion, respectively. In order to properly calculate these changes let us assume that the SSB radius vector of each star is given by $\mathbf{R} = \mathbf{R}_0 + \delta\mathbf{R}$, where $\delta\mathbf{R} = \delta\mathbf{R}_\perp + \delta\mathbf{R}_\parallel$ is decomposed into parallel and perpendicular to $\mathbf{S}_0$ components, respectively. Then, it can be shown that the first and second order corrections of direction are following

$$\delta\mathbf{S}^{(1)} = \frac{1}{\|\mathbf{R}_0\|}\delta\mathbf{R}_\perp, \qquad \delta\mathbf{S}^{(2)} = -\frac{1}{2}\left(\frac{\|\delta\mathbf{R}_\perp\|}{\|\mathbf{R}_0\|}\right)^2 \mathbf{S}_0 - \frac{\|\delta\mathbf{R}_\parallel\|}{\|\mathbf{R}_0\|^2}\delta\mathbf{R}_\perp. \tag{4}$$

If the interferometer is located at $\mathbf{R}_{\mathrm{O}}(t)$ in SSB frame then the observed direction towards the star is $\mathbf{s}(t) = \mathbf{S}(t) + \mathbf{\Pi}(t)$, where $\mathbf{\Pi}(t) = \pi\mathbf{S}_0 \times (\mathbf{S}_0 \times \mathbf{R}_{\mathrm{O}}(t))$ is the parallactic displacement, and π is the parallax of the star.

Omitting many details we can write the first order general formula for the relative delay measurement in the following form.

$$D = D^0 + D^\mu\, t + \mathbf{D}^\pi \cdot \mathbf{R}_{\mathrm{O}}(t) + \mathbf{d}^{\mathrm{c}} \cdot \mathbf{R}^\star(t) + \epsilon, \tag{5}$$

where $D^0 = \mathbf{B} \cdot (\mathbf{S}_0^1 - \mathbf{S}_0^2)$, $D^\mu = \mathbf{B} \cdot \left(\pi_1 \mathbf{V}_T^1 - \pi_2 \mathbf{V}_T^2\right)$, $\mathbf{D}^\pi = \left[\pi_1 (\mathbf{B} \cdot \mathbf{S}_0^1)\mathbf{S}_0^1 - \pi_2 (\mathbf{B} \cdot \mathbf{S}_0^2)\mathbf{S}_0^2\right] - (\pi_1 - \pi_2)\mathbf{B}$, the indices $1, 2$ refer to the target and reference star respectively; $\mathbf{d}^{\mathrm{c}} = \pi_1(\mathbf{B} \cdot \mathbf{e}_\alpha, \mathbf{B} \cdot \mathbf{e}_\delta)$ and $\{\mathbf{e}_\alpha, \mathbf{e}_\delta, \mathbf{e}_r\}$ defines the local frame centered at point $\mathbf{S}_0$ of the celestial sphere. Above, we assumed that only the target star has companions and by $\mathbf{R}^\star(t)$ we denote its position in the barycentric frame of the system.

One can determine the relative position of the target and reference star using two interferometers or, as it is planned for SIM, by performing two measurements with one interferometer for two different orientations of its baseline. Here we assume that a single observation is done for two orthogonal baseline orientations $\mathbf{B}_1$ and $\mathbf{B}_2$. Thus a single observations is given as a two component vector $\mathbf{D} = (D_1, D_2)$ of the relative delays. Each component D_i has the form (5) where coefficients D_i^0, D_i^μ, $\mathbf{D}_i^\pi$ and $\mathbf{d}_i^{\mathrm{c}}$ are calculated with the formulae (5) and $\mathbf{B} = \mathbf{B}_i$, $i = 1, 2$ respectively. To simplify the exposition we assume also that $\mathbf{B}_1$ and $\mathbf{B}_2$ are parallel to $\mathbf{e}_\alpha$ and $\mathbf{e}_\delta$, respectively.

Assuming that the target star possesses a planetary system with N planets we can represent $\mathbf{R}^\star(t)$ as a multiple Fourier series with coefficients depending on elements of planets. Similarly, we can expand $\mathbf{R}_{\mathrm{O}}(t)$. Then we obtain the following representation of the model

$$\mathbf{D} = \widehat{\mathbf{D}}^0 + \widehat{\mathbf{D}}^\mu\, t + \sum_{k=1}^{\infty}\left[\widehat{\mathbf{C}}^{\pi,k}\cos(n_{\mathrm{O}}kt) + \widehat{\mathbf{S}}^{\pi,k}\cos(n_{\mathrm{O}}kt)\right] + \sum_{j=1}^{N}\sum_{k=1}^{\infty}\left[\widehat{\mathbf{C}}^{j,k}\cos(n_j kt) + \widehat{\mathbf{S}}^{j,k}\cos(n_j kt)\right], \tag{6}$$

where N denotes the number of planets, n_{O} and n_j denote the mean motion of SIM and j-th planet, respectively. The above form of parametrization of the model allows to apply FD method described in details in [3]. Using it we can determine proper motions of planets n_j and successive vectorial amplitudes $\widehat{\mathbf{C}}^{j,k}$ and $\widehat{\mathbf{S}}^{j,k}$. It can be shown that knowing two first amplitudes for $k = 1, 2$ we can determine orbital elements of planetary orbits provided that eccentricities are not too big. As a test with υ And two planetary system showed, this reconstruction of orbital elements is more precise than expected. Fig. 1 shows magnitudes of harmonics corresponding to each planet in this system and to parallactic motion. It is important to notice that for application of FD method harmonic expansion of parallax effect in (6) is not necessary. We made it to show only that it gives an effect similar to a planet around the target star.

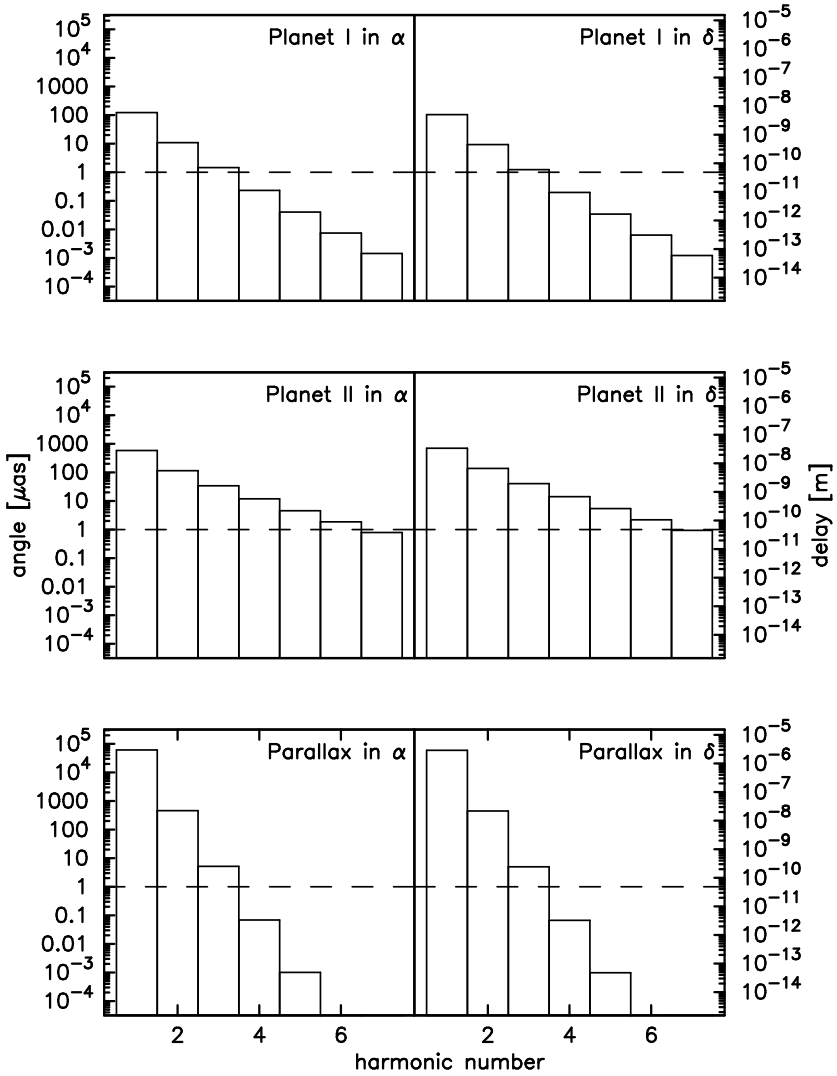

Figure 1: The amplitudes of subsequent harmonic terms for the relative delays D_1, D_2 (left and right panel respectively) corresponding to the planet I (a), II (b) and the parallactic motion (c).

2.1 Second order effects

The above first order model gives a good approximation for qualitative description of expected effects. However, SIM will deliver unprecedented 1μas precision in the narrow-angle mode and thus it is important to understand limitations of the model. It can be accomplished by analyzing higher order terms. For the baselines perpendicular to $\mathbf{S}_0$, the second order corrections correspond to the term that is responsible for the actual angular displacement (see equation (4)) and we have

$$\|\delta\mathbf{S}^{(2)}\| = \frac{\|\delta\mathbf{R}_\parallel\|}{\|\mathbf{R}_0\|}\frac{\|\delta\mathbf{R}_\perp\|}{\|\mathbf{R}_0\|} \le \left(\frac{\|\delta\mathbf{R}\|}{\|\mathbf{R}_0\|}\right)^2. \tag{7}$$

They can be calculated if we put $\delta\mathbf{R} = -\mathbf{R}_{\rm O}(t) + \mathbf{R}^\star(t) + \mathbf{R}_V(t)$ where $\mathbf{R}_V(t) = \mathbf{V}_T\,t + \mathbf{V}_R\,t$, and $\mathbf{V}_T$, $\mathbf{V}_R$ are the tangential and the radial velocity of the star. We obtain

$$\|\delta\mathbf{S}^{(2)}\| \le \pi^2\big(\|\mathbf{R}_{\rm O}(t)\|^2 + \|\mathbf{R}^\star(t)\|^2 + \|\mathbf{R}_V(t)\|^2 - \,2\,\mathbf{R}_{\rm O}(t)\cdot\mathbf{R}^\star(t) - 2\,\mathbf{R}_{\rm O}(t)\cdot\mathbf{R}_V(t) + 2\,\mathbf{R}^\star(t)\cdot\mathbf{R}_V(t)\big).$$

As we can see there are two types of second order corrections. The first type includes the second order corrections due to the proper motion, parallax and companions. For the proper motion it is easy to obtain the exact value of the correction

$$\Delta S_\mu = \frac{1}{4}\frac{\|\mathbf{V}_T\|}{\|\mathbf{R}_0\|}\frac{\|\mathbf{V}_R\|}{\|\mathbf{R}_0\|}\,\Delta T^2 = \frac{\pi^2}{4}\,V_T\,V_R\,\Delta T^2, \tag{8}$$

where ΔT is the time span of the mission. We calculated its value for the sample of 150 stars from the Hipparcos catalogue with the largest proper motion. The results are shown in Fig. 2. As one can see ΔS_μ is indeed significant for such stars and without any doubt has to be included into the model. For the remaining corrections due to the motion of the interferometer (i.e. the second order parallactic correction) and the presence of a companion we have the following upper limits

$$\begin{aligned}
\Delta S_{\rm c} &\approx 5\times10^{-6}\,\frac{m_{M_{JUP}}^2 P_{yr}^{4/3}}{d_{pc}^2 M_{M_\odot}^{4/3}(1-e)^2}\,\mu as \quad \text{for planetary companions,}\\
\Delta S_{\rm c} &\approx 4.9\frac{m_{M_\odot}^2 P_{yr}^{4/3}}{d_{pc}^2 M_{M_\odot}^{4/3}(1+m_{M_\odot}/M_{M_\odot})^{4/3}(1-e)^2}\,\mu as \quad \text{for stellar companions,}\\
\Delta S_\pi &\approx 4.9\,d_{pc}^{-2}\,\mu as,
\end{aligned} \tag{9}$$

where d_{pc} is the distance to the star in parsecs, $M_{M_\odot}$ mass of the star in solar masses, $m_{M_\odot}$ mass of the companion in solar masses, $m_{M_{JUP}}$ mass of the companion in Jupiter masses, P_{yr} orbital period in years and e eccentricity, $a_\star$ and $e_\star$ are the semi-major axis of the star's orbit and its eccentricity, respectively. Above we assume that SIM semi-major axis is 1 AU. The other type of second order corrections includes all "mixed" terms. We find that

$$\begin{aligned}
\Delta\Pi_{\rm c} &\approx 9\times10^{-3}\,\frac{m_{M_{JUP}} P_{yr}^{2/3}}{d_{pc}^2 M_{M_\odot}^{2/3}(1-e)}\,\mu as \quad \text{for planetary companions,}\\
\Delta\Pi_{\rm c} &\approx 9.7\frac{m_{M_\odot} P_{yr}^{2/3}}{d_{pc}^2 M_{M_\odot}^{2/3}(1+m_{M_\odot}/M_{M_\odot})^{2/3}(1-e)}\,\mu as \quad \text{for stellar companions,}
\end{aligned} \tag{10}$$

and

$$\begin{aligned}
\Delta\Psi_{\rm c} &\approx 0.1\,V_{100}\Delta T_{yr}\,\frac{m_{M_{JUP}} P_{yr}^{2/3}}{d_{pc}^2 M_{M_\odot}^{2/3}(1-e)}\,\mu as \quad \text{for planetary companions,}\\
\Delta\Psi_{\rm c} &\approx 102.3\,V_{100}\Delta T_{yr}\,\frac{m_{M_\odot} P_{yr}^{2/3}}{d_{pc}^2 M_{M_\odot}^{2/3}(1+m_{M_\odot}/M_{M_\odot})^{2/3}(1-e)}\,\mu as, \quad \text{for stellar companions,}
\end{aligned} \tag{11}$$

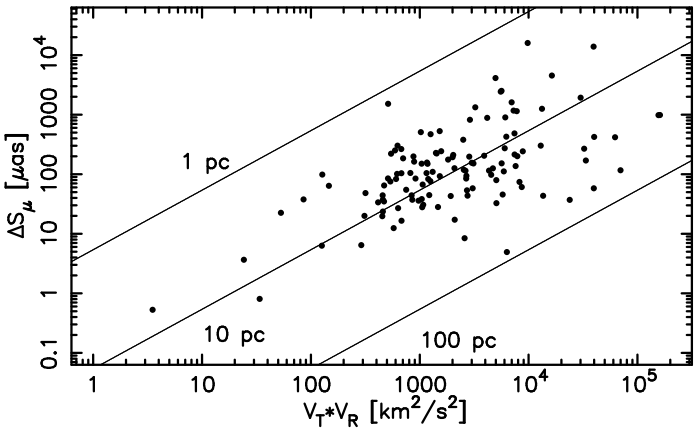

Figure 2: ΔS_μ for 150 stars with the largest proper motion from the Hipparcos catalogue. The solid lines represent ΔS_μ for 1, 10 and 100 parsecs as a function of $V_T\, V_R$. Time span of the mission $\Delta T = 10yr$ was assumed.

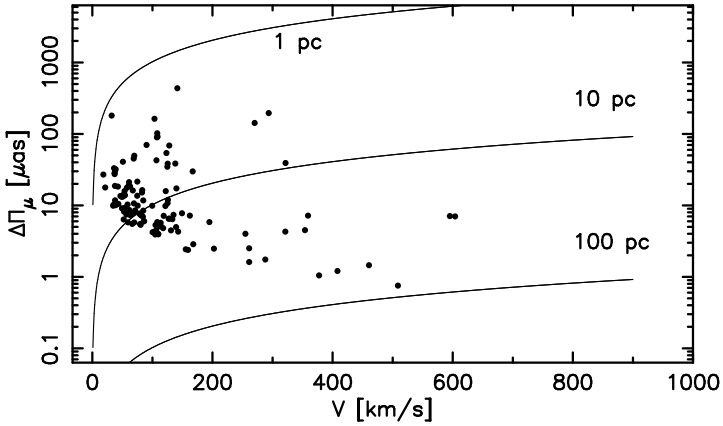

Figure 3: $\Delta\Pi_\mu$ for 150 stars with the largest proper motion from the Hipparcos catalogue. The solid lines represent $\Delta\Pi_\mu$ for 1, 10 and 100 parsecs as a function of V. Time span of the mission $\Delta T = 10yr$ was assumed.

where V_{100} is the velocity of star in hundreds of km/s and ΔT_{yr} is the time span of the mission in years; $\Delta\Pi_c$, $\Delta\Psi_c$ are upper limits of $2\pi^2\,|\mathbf{R}_O(t)\cdot\mathbf{R}^\star(t)|$ and $2\pi^2|\mathbf{R}^\star(t)\cdot\mathbf{R}_V(t)|$, respectively. The upper limit for mixed second correction due to parallax and proper motion is $\Delta\Pi_\mu = \pi^2 a_O V \Delta T$. The value of $\Delta\Pi_\mu$ was calculated for the same sample of stars as in Fig. 2. Again, one can observe that $\Delta\Pi_\mu$ is significant and a proper model has to take it into account (see Fig. 3). We estimated also the third order angular displacement $\delta S^{(3)}$ due to the proper motion. It is given by $\delta S^{(3)} \sim \frac{\pi^3}{8}(V_R^2 + V_T^2)^{3/2}\,\Delta T^3$, and is bigger than 1μ for several stars with big proper motions. The global second order effects on delays are illustrated in Fig. 4.

The above analysis clearly shows that a variety of second order effects and possibly in few cases third order effects will be detectable with SIM.

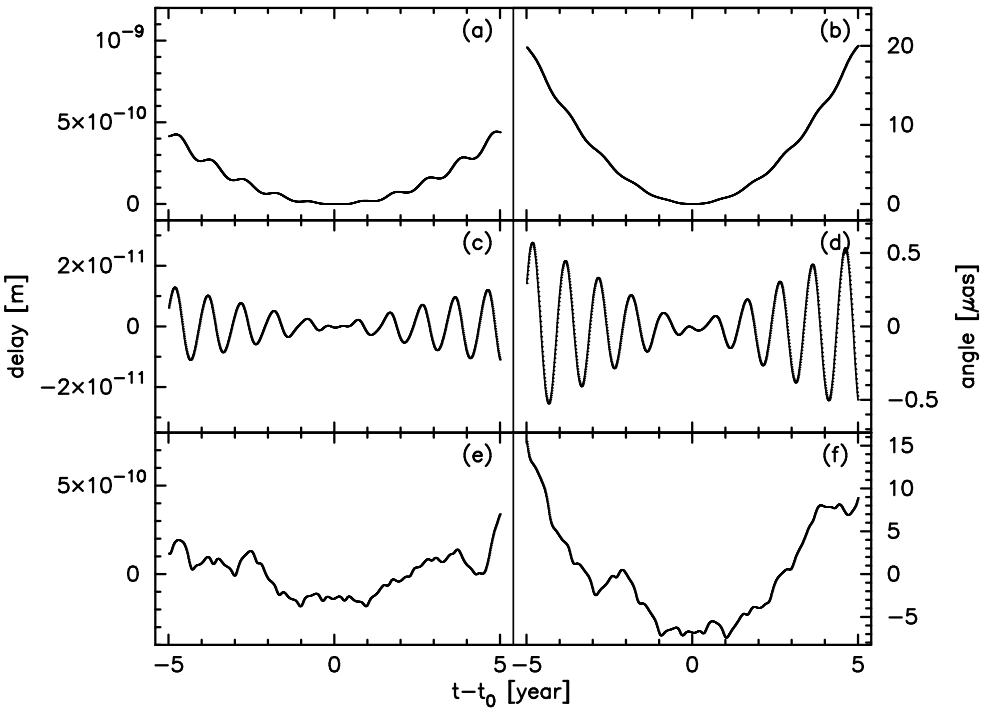

Figure 4: Second order effects in the simulated delays for the relative measurements between υ And and HD 10032 for the baseline vector orientations $\mathbf{B}_1$ (*a*) and $\mathbf{B}_2$ (*b*); (*c,d*) the same effects when the radial velocity of both stars is zero; (*e,f*) the residuals from the least-squares fit of the first order model to the simulated data used in (*a,b*).

References

[1] M. Konacki and A. J. Maciejewski. Frequency analysis and extra-solar planets. In J.-M. Mariotti and D. Alloi, editors, *Planets Outside the Solar System: Theory and Observations*, NATO Science Series C, pages 249–260, 1999.

[2] M. Konacki and A. J. Maciejewski. Frequency analysis of reflex velocities of stars with planets. *Astrophys. J.*, 518(1):442–449, 1999.

[3] M. Konacki, A. J. Maciejewski, and A. Wolszczan. Resonance in PSR B1257+12 planetary system. *Astrophys. J.*, 513(1):471–476, 1999.

[4] M. Konacki, A. J. Maciejewski, and A. Wolszczan. Frequency decomposition of astrometric signature of planetary systems. *Astrophys. J.*, 2000. submitted.

[5] M. Shao and R. Baron. The practice of astrometry in space with the space interferometry mission instrument. In *ASP Conf. Ser. 194: Working on the Fringe: Optical and IR Interferometry from Ground and Space*, pages 107+, 1999.

Atmospheric OPD implications for adaptive IR and optical interferometry

B. Femenía, M. Carbillet, S. Esposito, A. Riccardi

Osservatorio Astrofisico di Arcetri, Largo E. Fermi 5, 50125 Firenze, Italy

ABSTRACT

We present the concept of piston angular anisoplanatism and derive the temporal evolution of the optical path differences between the two pupils of an astronomical interferometer due to random fluctuations of the atmospheric refraction index, obtaining expressions for the temporal power spectra of phase fluctuations caused by differential piston and photon noise. This allows us to evaluate the residual phase variance left in a fringe tracking servo-loop system and obtain estimates for the sky-coverage due exclusively to differential piston effects, concluding that in the V-band the percentage of sky that can be observed is a few percent while in the K-band we should be able to cover the entire sky.

1. INTRODUCTION

For a long time it has been recognized that optical path differences originated from random fluctuations of the atmospheric index of refraction may cause a fringe displacement which if not corrected can completely blur and cancel out the visibility function. Thus, current small-aperture interferometers in operation already incorporate active fringe tracking systems which use the science object to track the fringes. These interferometers are very limited in sky-coverage due mainly to their small apertures which impose rather strong constraints on the limiting magnitude (m_v =5-7). On the other side, their small apertures of the order or r_0 makes non compulsory the use of adaptive optics. This situation is completely different for the new generation of optical ground-based interferometers[1–3] with apertures of 8-m and 10-m diameter and adaptive optics systems to correct from atmospheric degradation before cophasing the wavefronts from each single aperture. However, whereas tip-tilt and higher-order atmospheric effects have been studied in detail (e.g see Ref. 4–6) the effects of atmospheric differential piston on adaptive optics interferometry have been somehow overlooked and rarely found in the literature.[7,8]

2. EFFECT OF THE DIFFERENTIAL PISTON ON THE VISIBILITY

Let us assume an ideal situation where random fluctuations of the atmospheric refractive index distort the incoming wavefront by introducing a constant offset but of different values on the portions of wavefronts intercepted by each of the pupils of an astronomical interferometer*. Assuming identical atmospheric transmissions up to the two interferometers and along its two arms, the fringe pattern on the image plane is given by:

$$I(\vec{r}) \;=\; 2\, I_{DL}(\vec{r})(1 + V\cos(\phi(\tau) - \phi_{DP})) \tag{1}$$

where $\vec{r}$ is a vector on the image plane, I_{DL} is the diffraction limited pattern due to a single aperture (i.e. an Airy disk if we assume circular apertures), V is the instant visibility, ϕ_{DP} the phase caused by the differential piston (and therefore the DP subscript) and $\phi(\tau)$ the phase due to both spatial and temporal coherence. Once we have selected the point of observation in the image plane $\phi(\tau)$ has a constant value so that the averaged visibility $\tilde{V}$ will differ from the instant visibility due to temporal changes of ϕ_{DP}. Assuming that ϕ_{DP} behaves as a Gaussian random variable with variance σ_ϕ^2 it can be readily found that the time average visibility function $\tilde{V}$ is given by::

$$\tilde{V} \;=\; V\exp(-\frac{\sigma_\phi^2}{2}) \tag{2}$$

*The difference of these offsets is referred to as differential piston in what follows.

3. DIFFERENTIAL PISTON ANGULAR ANISOPLANATISM

The loss of correlation between the differential piston when looking towards the on-axis science object and the differential piston measured from an off-axis bright reference source translates in a residual phase difference referred to as differential piston angular anisoplanatism. Adopting the same terminology as in Ref. 9 we consider an interferometer made up of two pupils of diameter D and a center-to-center distance (i.e baseline) equal to Δ. The instrument is assumed to be pointing towards zenith and observing an on-axis scientific target while correcting for differential piston by observing a bright reference source at an off-axis angle θ. Further, consider an atmosphere with a Von Karman power spectrum with outer scale L_0, all turbulent power concentrated in a single layer at an altitude h above the interferometer and a Fried parameter r_0 at the observing wavelength λ. Referring to Fig. 1-left for the definition of the geometrical elements s, d_{12} and d_{21}, it can be shown that the phase variance due to differential piston angular anisoplanatism $(\sigma_\phi)^2_{ani}$ is given by:

$$(\sigma_\phi)^2_{ani} = 0.3664\,\pi^{8/3}\left(\frac{D}{r_0}\right)^{5/3}\int_0^\infty \frac{2\left[1-J_0\left(2x\frac{s}{D}\right)-J_0\left(2x\frac{\Delta}{D}\right)\right]+J_0\left(2x\frac{d_{12}}{D}\right)+J_0\left(2x\frac{d_{21}}{D}\right)}{x\left[x^2+\left(\pi\frac{D}{L_0}\right)^2\right]^{11/6}}J_1^2(x)\,\mathrm{dx} \qquad (3)$$

In Fig. 1-right we show the behavior of the anisopistonic optical path difference rms $(\sigma_{\rm p})_{ani} = 2\pi\,(\sigma_\phi)_{ani}/\lambda$ for an LBT-like configuration ($D = 8.4$ m, $\Delta = 14.4$ m) due to a single turbulent layer with $r_0(0.55\mu\mathrm{m}) = 0.2$ m at $h = 10$ km above the telescope for several L_0 values.

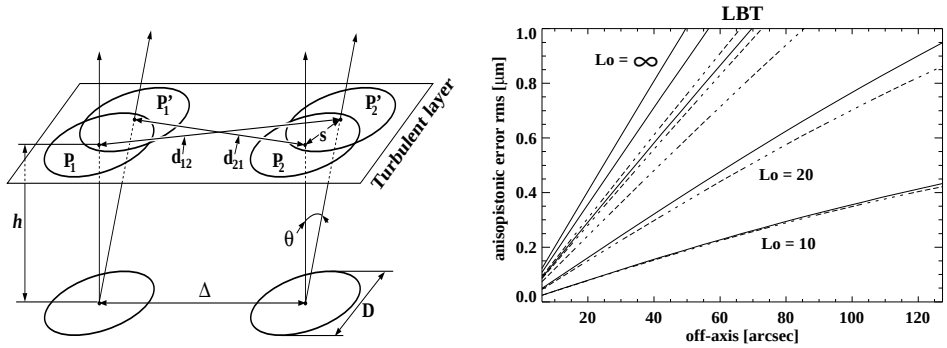

Figure 1. Left: geometrical elements considered for the calculations of phase variance due to differential piston angular anisoplanatism. **Right:** anisopistonic optical path difference rms $(\sigma_{\rm p})_{ani}$ as a function of the off-axis angle of the reference source for a single-layer turbulent atmosphere (see text for the details on the rest of parameters). Plotted curves refer to $L_0 = 10$, 20, 50, 100 m and ∞ from the least to the steepest curve. Solid and dotted lines represent the cases where the reference source is displaced along and orthogonally to the baseline, respectively.

4. SERVO-LOOP DELAY EFFECTS

The second source of differential piston phase residuals in an adaptive optics interferometer is due to the fact that the correction is applied with a certain delay during which little changes are expected to occur. In order to estimate the contribution from this source to the total differential piston variance we must first compute the temporal power spectrum of the differential piston. Once such temporal power spectrum is obtained, the temporal behavior of phase residuals in our servo-loop is obtained by considering the servo-loop transfer function.

4.1. Temporal Power Spectrum of Differential Piston Phase Fluctuations

To do so we have first obtained the temporal auto-covariance function of the differential piston under rather general assumptions, namely: Taylor hypothesis and spatial isotropy of the field of random atmospheric refractive index

fluctuations[†]. After obtaining the temporal auto-covariance we are ready to find the temporal power spectrum by just applying the Wiener-Khinchin theorem. Assuming a Von Karman spectrum to model the random fluctuations of the atmospheric index of refraction, the expressions for the temporal power spectra corresponding to the cases of wind parallel and perpendicular to our interferometer baseline are:

$$\Gamma_\phi^{\parallel}(f) = \frac{0.6202}{\lambda^2 D^2} \sec\psi \, f^{-\frac{14}{3}} \int_0^\infty \mathrm{dh}\, \mathrm{C_n^2(h)}\, v(\mathrm{h})^{\frac{11}{3}}\, \mathrm{F}^{\parallel}\left(\frac{\mathrm{f}}{v(\mathrm{h})}\,;\, \mathrm{D},\, \mathrm{L_0}\right) \left[1 - \cos\left(\frac{2\pi\Delta}{v(\mathrm{h})}\mathrm{f}\right)\right] \tag{4}$$

$$\Gamma_\phi^{\perp}(f) = \frac{0.6202}{\lambda^2 D^2} \sec\psi \, f^{-\frac{14}{3}} \int_0^\infty \mathrm{dh}\, \mathrm{C_n^2(h)}\, v(\mathrm{h})^{\frac{11}{3}}\, \mathrm{F}^{\perp}\left(\frac{\mathrm{f}}{v(\mathrm{h})}\,;\, \mathrm{D},\, \Delta,\, \mathrm{L_0}\right) \tag{5}$$

where ψ is the zenith angle, D the aperture diameter, Δ the interferometer baseline, $C_n^2(h)$ and $v(h)$ the structure *constant* of the refractive index fluctuations and wind velocity at height h, respectively, and $F^{\parallel}$ and $F^{\perp}$ are defined according to the following integrals:

$$F^{\parallel}(y\,;\, D,\, \Delta,\, L_0) = \int_0^1 \mathrm{dx}\, \frac{\mathrm{x}^{\frac{11}{3}}}{\sqrt{1-\mathrm{x}^2}} \left[1 + \left(\frac{\mathrm{x}}{\mathrm{y\,L_0}}\right)^2\right]^{\frac{-11}{6}} \mathrm{J}_1^2\left(\frac{\pi\,\mathrm{D}}{\mathrm{x}}\,\mathrm{y}\right) \tag{6}$$

$$F^{\perp}(y\,;\, D,\, \Delta,\, L_0) = \int_0^1 \mathrm{dx}\, \frac{\mathrm{x}^{\frac{11}{3}}}{\sqrt{1-\mathrm{x}^2}} \left[1 + \left(\frac{\mathrm{x}}{\mathrm{y\,L_0}}\right)^2\right]^{\frac{-11}{6}} \mathrm{J}_1^2\left(\frac{\pi\,\mathrm{D}}{\mathrm{x}}\,\mathrm{y}\right) \left[1 - \cos\left(\frac{2\pi\Delta}{\mathrm{x}}\mathrm{y}\sqrt{1-\mathrm{x}^2}\right)\right] \tag{7}$$

In Conan et al.[8] the authors provide the expression of the temporal power spectrum of differential piston phase fluctuations but in the more simple case of a Kolmogorov spectrum and wind parallel to baseline. Our expression for $\Gamma_\phi^{\parallel}$ reduces to theirs for the parallel case with a single layer and $L_0 \to \infty$. Additionaly we have tested our results by comparing against simultaions conducted with LA^{3}OS^2 code.[10] We conclude this section by remarking the fact that considering the particular parallel and perpendicular cases removes no generality as far as we can always express the differential piston phase power spectrum for any wind direction in terms of $\Gamma_\phi^{\parallel}(f)$ and $\Gamma_\phi^{\perp}(f)$. To do this in addition of a vertical wind speed profile we must also consider the vertical profile of wind directions $\theta(h)$ with respect to the interferometer baseline.

4.2. Convolving with the Servo-loop Transfer Function

We assume the servo-loop of an adaptive fringe tracking system as made of a correcting element (i.e. delay line), a fringe sensor, an integrator and a feedback element to close the loop. In our calculations we assume a correcting element fast enough not to introduce any significant delay in the correction so that we can approximate $H_c(f) = 1$. The transfer function for the fringe sensor $H_s(f)$ takes into account the integration time τ plus the delay associated to it, so it is described by (e.g. see Ref. 6) $H_s(f) = (1 - \exp(-j2\pi f\tau))/(j2\pi f\tau)$. We consider a pure integrator with transfer function $H_i(f) = 1/(j2\pi f\tau)$ and a unit feedback element (i.e. $H_f(f) = 1$). The residual differential piston phase rms σ_ϕ in the servo-loop system is given by:

$$(\sigma_\phi^2)_\tau = 2\int_0^\infty \mathrm{df}\, |\mathrm{T}_\phi(\mathrm{f})|^2\, \Gamma_\phi(\mathrm{f}) \tag{8}$$

where the subscript τ makes reference to the integration time and $|T_\phi(f)|^2$ is the square modulus of the servo-loop error-input transfer function given by (e.g. see Ref. 6):

$$|T_\phi(f)|^2 = \left|\frac{1}{1 + H_s(f)H_i(f)}\right|^2 = \frac{(2\pi f\tau)^4}{(2\pi f\tau)^4 - 4\sin^2(\pi f\tau)\,[(2\pi f\tau)^2 - 1]} \simeq \frac{(2\pi f\tau)^2 + \frac{4}{89}(2\pi f\tau)^4}{1 + \frac{2}{45}(2\pi f\tau)^4} \tag{9}$$

[†] The Taylor hypothesis, or frozen turbulence approximation, assumes that each turbulent layer moves rigidly without changing its shape. By adopting this hypothesis we can directly link time variations of any quantity related to the wavefront with its spatial variations.

Performing the integration involved in Eq. 8 with $|T_\phi(f)|^2$ and $\Gamma_\phi(f)$ given by Eq. 9, Eq. 4 and Eq. 5 is an extremely cumbersome task. Therefore we proceed by using approximate expressions for the error-input transfer function in close-loop operation and instead of Eq. 4 and Eq. 5 we make use of the asymptotic behaviours of $\Gamma_\phi^{\parallel}(f)$ and $\Gamma_\phi^{\perp}(f)$ in Ref. 11. Now the integration in Eq. 8 can be readily done to obtain the residual differential piston phase variance according to the expression:

$$(\sigma_\phi^2)_\tau \;=\; A_0\,\sec\psi\,\left(\frac{2\pi}{\lambda}\right)^2\,D^{-1/3}\,\tau^2\,\left\{(1+A_1)\,v_2\;+\;\int_0^\infty \mathrm{dh}\,\mathrm{C_n^2(h)}\,v^2(h)\,\left[A_2\cos^2\theta(h)\;+\;A_3\sin^2\theta(h)\right]\right\} \tag{10}$$

where let us recall that τ is the integration time, $v_2 \;=\; \int_0^\infty \mathrm{dh}\,\mathrm{C_n^2(h)}\,v^2(h)$ is the 2nd order velocity moment and where for a Kolmogorov spectrum (i.e. $L_0=\infty$): $A_0=5.81$, $A_1=0$, $A_2-0.69(D/\Delta)^{1/3}$ and $A_3=-0.16(D/\Delta)^{1/3}$. For finite outer scales $A_0=0.643$ and:

$$A_1 \;=\; \left\{\begin{array}{ll} 0 & \text{if } L_0 \;<\; \frac{3}{2}\,D \\ 3.61\times10^{-2}\,(L_0/D)^{8/3}\;{}_2F_1(4/3,3/2;5/2;-0.09(L_0/D)^2) & \text{if } L_0 \;>\; \frac{3}{2}\,D \end{array}\right. \tag{11}$$

$$A_2 \;=\; \left\{\begin{array}{ll} 3.61\times10^{-2}(L_0/D)^{8/3}\left[\;{}_2F_1(4/3,3/2;5/2;-0.09(L_0/D)^2)+9.02\times10^{-2}(L_0/\Delta)\right]\;- & \\ 1.07\times10^{-2}(L_0/\Delta)^{8/3}\;{}_2F_1(4/3,3/2;5/2;-0.04(L_0/\Delta)^2) & \text{if } L_0 \;<\; \frac{3}{2}\,D \\ & \\ -1.07\times10^{-2}(L_0/\Delta)^{8/3}\left(1-0.474(D/\Delta)^{1/3}\right)\;{}_2F_1(4/3,3/2;5/2;-0.04(L_0/\Delta)^2) & \text{if } L_0 \;>\; \frac{3}{2}\,D \end{array}\right. \tag{12}$$

$$A_3 \;=\; \left\{\begin{array}{ll} 2.31\times10^{-2}(L_0/D)^{11/3} & \text{if } L_0 \;<\; \frac{3}{2}\,D \\ -8.31\times10^{-2}\,(L_0/D)^{8/3}\gamma(3/2,3\Delta^2/(4D^2))\exp(-8.32\Delta^2/L_0^2) & \text{if } L_0 \;>\; \frac{3}{2}\,D \end{array}\right. \tag{13}$$

5. DETECTOR NOISE EFFECTS

The last source under consideration of residual differential piston phase is that generated by photon noise in our fringe tracking sensor. A recent work[12] suggests the fact that current working interferometers are still detector-noise limited, or at least that the detector-noise contribution is not negligible at all. Yet in our approach we consider only photon-noise as far as our analysis is to be applied to Michelson interferometers with very large pupils. We have adopted the phase-tracking method described in Ref. 13 and the reader is referred to that work for details on it. According to Ref. 13 the expected phase variance under photon-noise limited (and hence the subscript pn) wide-band fringe tracking is given by $(\sigma_\phi)^2_{pn} \;=\; \pi^2/(4\,V^2\,N)$ where V is the visibility and N is the number of detected photo-electrons and implicitly contains time and wavelength bandwidth dependences. Assuming white photon-noise and that it passes through a boxcar averager with time constant τ we can write:

$$\Gamma_{pn}(f) \;=\; \tau\,(\sigma_\phi)^2_{pn} \;=\; \frac{\pi}{\eta\,V^2\,D^2}\,10^{0.4m-10}\,\left(\frac{100\mathrm{nm}}{\Delta\lambda}\right) \tag{14}$$

where $\Gamma_{pn}(f)$ is the power spectrum associated with the photon noise in terms of the two pupil collecting surface $2\,D$ (D in units of [m]), the quantum efficiency of the fringe sensor η, the magnitude m of the reference star and the bandwidth $\Delta\lambda$ of the sensing light. The transfer function T_{pn} we must use with Γ_{pn} is, according to Ref. 6, the overall transfer function of the closed loop as it is assumed that the noise in the device enters through the fringe sensor and propagates across the integrator and feedback elements:

$$|T_{pn}\,(f)|^2 = \left|\frac{H_s(f)H_i(f)}{1\;+\;H_s(f)H_i(f)}\right|^2 \;\simeq\; \frac{1}{1+(2\pi f\tau)^4/12} \tag{15}$$

The residual variance due to the presence of photon noise $(\sigma_\phi^2)_{pn}$ within the servo system is then readily evaluated to be:

$$(\sigma_\phi^2)_{pn} \;=\; 2\int_0^\infty \mathrm{df}\,|\mathrm{T_{pn}(f)}|^2\,\Gamma_{\mathrm{pn}}(\mathrm{f}) \;=\; \frac{3^{1/4}\,\pi\,10^{0.4\mathrm{m}-10}\,\left(\frac{100\mathrm{nm}}{\Delta\lambda}\right)}{2\,\eta\,\mathrm{V^2\,D^2}\,\tau} \tag{16}$$

6. APPLICATION: SKY COVERAGE FOR 8M-CLASS INTERFEROMETERS

We consider the configurations corresponding to Keck ($D = 10$m, $\Delta = 85$m), LBT ($D = 8.4$m, $\Delta = 14.4$m), VLTI UT1-UT2 ($D = 8.2$m, $\Delta = 57$m) and VLTI UT1-UT4 ($D = 8.2$m, $\Delta = 130$m). For Keck and VLTI we use available SCIDAR measurements for the atmospheric turbulence profiles above Mauna Kea[14] and Cerro Paranal.[15] In absence of atmospheric turbulence profiles for LBT we have considered a modified Hufnagel-Valley model.[6] These atmospheric turbulence profiles have been normalized to the median $r_0(0.5\mu\text{m})$ values above each site: 20.4, 13.3 and 14.1 cm for the Keck,[14] LBT[16] and VLTI,[17] respectively . Wind profiles in Ref. 15 and Ref. 18 are used for Keck and VLTI and due to the absence of such data for LBT, we assume the standard Bufton wind model with ground wind speed set to 5 m/s. Finally, to our knowledge there is no vertical θ profile so that we will assume a uniformly random wind direction profile along the atmosphere. In the same manner as we define the concepts of anisoplanatic angle and the high-order critical time constant we define the isopistonic angle $\theta_{\rm P}$ and the pistonic critical time $\tau_{\rm P}$. Thus, we define $\theta_{\rm P}$ as the angular radius of a circular region where the anisopistonic error reduces the fringe visibility to no more than 80% of the unperturbed value. The 20% visibility reduction happens when the residual piston error $\sigma_{\rm p}$ is about $\lambda/10$. The pistonic critical time $\tau_{\rm P}$ is defined as the value at which $(\sigma^2_\phi)_\tau = 1$rad implying a $\sim$40% fringe visibility reduction. Following Ref. 6 the fractional sky coverage and the density number of stars of visual magnitude less or equal to m_v) are given by:

$$\begin{aligned} \text{fractional sky coverage} &= \pi\vartheta^2 \times (\text{average star density})_{m_v} \\ (\text{average star density})_{m_v} &= 1.45\,\exp(0.96\,m_v) \quad (\text{stars/rad}^2) \end{aligned} \tag{17}$$

where ϑ is the angular radius around the reference source within which the isopistonic error reduces the visibility by a tolerable value. The limiting magnitude m_v will be determined by the trade-off between the maximum integration time before $(\sigma^2_\phi)_\tau$ degrades V and the minimum required time beyond which $(\sigma^2_\phi)_{pn}$ preserves V to its desired value. Considering that in addition to the fringe visibility caused by differential piston there will be other sources of visibility reduction (e.g. differential tilt, high-orders correction effects, finite bandwidth, etc) we find appropriate to set our goal to achieve a visibility reduction of 50% due to differential piston. Taking $\vartheta = \theta_{\rm P}$ leaves a budget of 0.94 rad^2 to be distributed between $(\sigma^2_\phi)_\tau$ and $(\sigma^2_\phi)_{pn}$ of which we arbitrarily allocate a 90% to the former and a 10% to the latter. This arbitrary allocation yields integration times for the fringe sensor ranging from $\sim$6 ms to $\sim$10 ms. From here we proceed by assuming a fringe detector with a total throughput of 40% and sensing done in the V-band. The value for the limiting magnitude in the V-band together with the expected fractional sky coverage values are also provided in Table 1. Thus, while in the V-band the expected sky coverage is only a few per cent, in the K-band we should be able to cover the entire sky.

Table 1. Summary of the parameters and results of the estimates on sky coverage.

Interferometer	K-BAND		V-BAND			Sky Coverage	
	$\theta_{\rm P}$ [arcsec]	$\tau_{\rm P}$ [ms]	$\theta_{\rm P}$ [arcsec]	$\tau_{\rm P}$ [ms]	Limiting m_v	K-band (%)	V-band (%)
	$L_0 = 20$ m						
Keck	24.3	29.2	6.00	7.30	18.4	100	18
LBT	21.9	44.3	5.43	11.1	18.5	100	19
VLTI	27.1	70.4	6.68	17.6	18.6	100	44
	$L_0 = 50$ m						
Keck	13.0	25.0	3.24	6.25	18.4	72	4.5
LBT	13.4	39.1	3.33	9.78	18.5	84	5.2
VLTI	15.6	45.1	3.90	11.3	18.6	100	7.9

7. CONCLUSION

Our calculations on the effects of differential piston for adaptive optics interferometry show that the sky-coverage in the V-band is indeed quite small, while close to full coverage in the K-band. These results are very much dependent on the particular $C_n^2(h)$ and $v(h)$ profiles as well as on the outer scale. At this point we do not claim that a particular interferometer will be able to cover twice as much sky as the other since the profiles used for any of them have been obtained with very different resolutions thus affecting the exact sky-coverage values obtained. Instead, these values should be viewed as orders of magnitude so that we conclude that the new generation of optical ground-based interferometers should be able to cover the sky at a level of 20-40% in the V-band and at 100% in the K-band if only differential piston were present nd assuming $L_0 = 20$m, while for $L_0 = 50$ we still reach a 100% sky-coverage in the K-band while in the V-band we are limited to 5-10% sky coverage. Further considerations including the effects of residual tip-tilt correction between the two pupils (the so-called differential tilt) as well as residual higher-order corrections are likely to further constrain the sky-coverage of these interferometers, a question which should be studied in more detail.

REFERENCES

1. M. M. Colavita, A. F. Boden, S. L. Crawford, A. B. Meinel, M. Shao, P. N. Swanson, G. T. Van Belle, G. Vasisht, J. M. Walker, J. K. Wallace, and P. L. Wizinowich, "Keck interferometer," *Proc. SPIE* **3350**, pp. 776–784, July 1998.
2. J. M. Hill and P. Salinari, "Large binocular telescope project," *Proc. SPIE* **3352**, pp. 23–33, Aug. 1998.
3. J. M. Mariotti, C. Denise, F. Derie, M. Ferrari, A. Glindemann, B. Koehler, S. A. Leveque, F. Paresce, M. Schoeller, M. Tarenghi, and M. Verola, "Vlti program: a status report," *Proc. SPIE* **3350**, pp. 800–806, July 1998.
4. D. L. Fried, "Anisoplanatism in adaptive optics," *J. Opt. Soc. Am. A* **72**, pp. 52–61, Jan. 1982.
5. J. M. Beckers, "Adaptive optics for astronomy - principles, performance, and applications," *ARA&A* **31**, pp. 13–62, 1993.
6. R. R. Parenti and R. J. Sasiela, "Laser-guide-star systems for astronomical applications," *J. Opt. Soc. Am. A* **11**, pp. 288–309, Jan. 1994.
7. J. M. Mariotti, "Adaptive optics for long baseline optical interferometry," in *NATO Advanced Study Institute on Adaptive Optics for Astronomy*, D. M. Alloin and J. M. Mariotti, eds., pp. 309 – 320, Kluwer Academic Publishers, The Netherlands, 1994.
8. J. M. Conan, G. r. Rousset, and P. Y. Madec, "Wave-front temporal spectra in high-resolution imaging through turbulence," *J. Opt. Soc. Am. A* **12**, pp. 1559–1570, July 1995.
9. S. Esposito, A. Riccardi, and B. Femenía, "Differential piston angular anisoplanatism for astronomical optical interferometers," *A&A* **353**, pp. L29–L32, Jan. 2000.
10. M. Carbillet, B. Femenía, F. Delplancke, S. Esposito, L. Fini, A. Riccardi, E. Viard, N. N. Hubin, and F. J. Rigaut, "La^{3}os^2: a software package for laser guide star adaptive optics systems," *Proc. SPIE* **3762**, pp. 378–389, Sept. 1999.
11. B. Femenía, M. Carbillet, S. Esposito, and A. Riccardi, "Considerations about the differential piston for adaptive optics," *Proc. SPIE* **4006**, pp. 1116–1127, 2000.
12. M. M. Colavita, "Fringe visibility estimators for the palomar testbed interferometer," *PASP* **111**, pp. 111–117, Jan. 1999.
13. M. Shao and D. H. Staelin, "Long-baseline optical interferometer for astrometry," *Optical Society of America Journal* **67**, pp. 81–86, 1977.
14. R. Racine and B. L. Ellerbroek, "Profiles of nighttime turbulence above mauna kea and isoplanatism extension in adaptive optics," *Proc. SPIE* **2534**, pp. 248–257, Aug. 1995.
15. M. Sarazin, "Site atmospheric characterization," in *Topical Meeting on Adaptive Optics*, M. Cullum-ESO, ed., pp. 439–444, ESO, 1996.
16. B. L. Ulich and W. B. Davison, "Seeing measurements on mount graham," *PASP* **97**, pp. 609–615, July 1985.
17. M. Le Louarn, R. Foy, N. Hubin, and M. Tallon, "Laser guide star for 3.6- and 8-m telescopes: Performance and astrophysical implications," *MNRAS* **295**, pp. 756–768, Apr. 1998.
18. S. S. Olivier and D. T. Gavel, "Tip-tilt compensation for astronomical imaging," *J. Opt. Soc. Am. A* **11**, pp. 368–378, Jan. 1994.

Layer oriented approach to multiconjugation in Adaptive Optics

Massimiliano Tordi

Abstract

A new scheme for multiconjugation in adaptive optics is presented. This approach, proposed by Ragazzoni, Marchetti and Farinato, uses single detectors conjugated at the same altitude as the deformable mirrors. This solution results in a simple optical design, less expensive in terms of computing power, that can be easily managed by changing the integration time and the spatial sampling, in order to reach more faint limiting magnitudes and increase the sky coverage with natural guide stars.